Temperature effects on the electrohydrodynamic and electrokinetic behaviour of ion-selective nanochannels

2016 J. Phys.: Condens. Matter 28 114002

(http://iopscience.iop.org/0953-8984/28/11/114002)

OPEN ACCESS
IOP Publishing
Journal of Physics: Condensed Matter
J. Phys.: Condens. Matter **28** (2016) 114002 (9pp)
doi:10.1088/0953-8984/28/11/114002

Temperature effects on the electrohydrodynamic and electrokinetic behaviour of ion-selective nanochannels

Jeffery A Wood, Anne M Benneker and Rob G H Lammertink

Soft Matter, Fluidics and Interfaces, Mesa+Institute for Nanotechnology, University of Twente, 7500AE Enschede, The Netherlands

E-mail: r.g.h.lammertink@utwente.nl

Received 31 July 2015, revised 6 November 2015
Accepted for publication 9 November 2015
Published 23 February 2016

Abstract

A non-isothermal formulation of the Poisson–Nernst–Planck with Navier–Stokes equations is used to study the influence of heating effects in the form of Joule heating and viscous dissipation and imposed temperature gradients on a microchannel/nanochannel system. The system is solved numerically under various cases in order to determine the influence of temperature-related effects on ion-selectivity, flux and fluid flow profiles, as well as coupling between these phenomena. It is demonstrated that for a larger reservoir system, the effects of Joule heating and viscous dissipation only become relevant for higher salt concentrations and electric field strengths than are compatible with ion-selectivity due to Debye layer overlap. More interestingly, it is shown that using different temperature reservoirs can have a strong influence on ion-selectivity, as well as the induced electrohydrodynamic flows.

Keywords: ion-selectivity, temperature effects, electrokinetics

(Some figures may appear in colour only in the online journal)

1. Introduction

Ion-transport phenomena are at the foundation of many technical solutions in future water treatment and energy scenarios. With regards to energy generation or desalination, the transport of charge carriers other than the electrons can present a major challenge [1–3]. Desalination, via ion-selective membranes or other techniques, is of crucial importance in helping to address lack of access to fresh drinking water [4, 5], with numerous interesting phenomena relating to limiting and overlimiting current behaviour observed. The creation of ion-selective channels through the use of nanochannels, where the characteristic dimension is on the order of the Debye length, has been used as a model system for studying ion-transport phenomena as well as investigating other micro- and nanoscale phenomena. The advantage provided through the use of well-defined fabrication tolerances for characterizing resulting behaviour is clear compared to membranes, which typically possess larger pore-size distributions. Ion-selective nanochannels are well-established as an investigation platform [6–9] with many potential applications. These include: desalination [10], power generation via electrokinetic energy conversion or reverse electrodialysis [11–13] and particle separation through electric field enhancement in concentration depletion zones [14, 15]. The behaviour of such channels has been studied in depth both experimentally and theoretically, examining the degree of ion-selectivity, characterising the electrical properties such as conductance, surface charge or zeta potential [16, 17] or induced fluid flows due to local breaking of electroneutrality [18, 19]. Additionally, more practical applications have been formulated, ranging from the use of nanochannel arrays or networks to drive micromixing [20, 21] or acting as a highly sensitive sensor for characterizing protein adsorption [22].

In order to describe the transport of ions through a charged nanochannel, a number of theoretical frameworks have been employed. These range from simplified conductance models based on 1D analytical solutions of the Poisson–Boltzmann equation [23, 24] to numerical solution in 2D or 3D of the full balance equations to describe the transport of ions (Nernst–Planck equation), potential distribution (Poisson equation) and momentum (Navier–Stokes or Stokes flow) [7, 25]. The coupling of the ion distribution to the potential forms a non-linear PDE, which can be simplified by assuming a Boltzmann distribution for ions at the surface under the conditions of low surface potential and non-overlapping double layers. However, this assumption is of limited value for the case of an ion-selective nanochannel where double layer overlap is a requirement. In order to describe both the electrokinetic and electrohydrodynamic effects observed in a microchannel/nanochannel device, it is of crucial importance to account for entrance/exit effects from the nanochannel [9]. This is due to the large variation in hydrodynamic resistance between the micro and nanochannel, as well as constriction effects on any applied fields.

In comparison to the large breadth of experimental and theoretical work for ion-selective nanochannels under or assuming isothermal conditions, the role of temperature, and more specifically, temperature gradients is relatively unexplored. Investigation has focused primarily on heat transfer in charged microchannels and the role this plays in induced electroosmotic flows. For example, Chen (2009) studied the development of temperature profiles in micro- and nanochannels with a thin double layer at low potentials using a Poisson–Boltzmann framework considering Joule heating (JH) as the primary heat source while neglecting viscous dissipation based on order of magnitude considerations [26]. The results demonstrated the importance of temperature on the resulting electroosmotic flow (EOF) and friction factors for pure EOF, as well as EOF with pressure gradients, finding that viscous dissipation became comparable to JH for channels smaller than 50 nm [26]. This work also demonstrated the importance of accounting for the temperature-dependence of physical properties, as significant deviations could be observed assuming a constant value. Shi *et al* (2008) used the Lattice-Boltzmann method to describe non-isothermal electroosmotic flows again with a Poisson–Boltzmann type distribution, concluding that for channels less than 100 nm in diameter viscous dissipation effects will become dominant compared with JH, dependent upon the salt concentration in the bulk [27].

The role of temperature gradients in the double layer and how this coupled to thermoelectric effects was studied theoretically recently by Ghonge *et al* [28], using a Poisson–Nernst–Planck approach, indicating that Soret and thermoelectric effects could be significant for the case of electrohydrodynamic flow in a nanochannel with an imposed wall temperature gradient along the channel axis. The contribution of JH was neglected versus viscous dissipation based on an order of magnitude analysis, although in a micro/nanojunction system the electric field constriction and enhancement due to cation or anion depletion/enrichment may result in conditions where the Joule heat contribution could be significant. However, the role of temperature effects in nanochannels on the resulting ion-selectivity, fluxes and induced flow profiles in the case of double layer overlap or high surface charges/wall potentials has not been examined in depth.

It is the aim of this study to numerically investigate the effects of temperature on the resulting electrokinetic and electrohydrodynamic behaviour of nanochannels. In particular, the region with high surface potentials/surface charges and large overlap of the double layer is of interest, as the role of imposed temperature gradients, viscous dissipation, Joule heating, etc for charge-selective nanochannels has not yet been explored in detail. In order to accomplish this goal, a theoretical framework based on a non-isothermal formulation of the Poisson–Nernst–Planck equations, Navier–Stokes and energy balance has been formulated in order to determine the couplings between temperature, ion-species concentration, fluid velocity and electrical potential. Using this framework, numerical simulations were undertaken to investigate the role of temperature effects on ion-selectivity, flux and induced fluid flows.

2. Theoretical background

2.1. Dimensionless non-isothermal Poisson–Nernst–Planck with Navier–Stokes

In order to simulate the influence of various temperature-related effects on transport in ion-selective media, a model framework based on a non-isothermal formulation of the steady-state Poisson–Nernst–Planck (PNP) equations coupled with the Navier–Stokes was formulated. This framework (or variations) have been employed successfully by a number of authors to describe the resulting ion-transport, induced fluid-flows (electroosmotic and otherwise), etc [29–31]. Depending on the salt concentration, significant deviations from assuming Poisson–Boltzmann (PB) type behaviour can be expected, which motivates the use of a non-equilibrium approach such as PNP [25, 29]. The total channel height considered was 20 nm, which also corresponds to experimental conditions [32], additionally these geometric dimensions have been considered numerically for isothermal simulations of nanochannels [25, 33] and allow for treating the system as a continuum [34]. The equations were scaled for numerical and comparison purposes.

The electrical potential in the system was split into two contributions: the applied potential, φ, and the induced electrokinetic potential, ψ, as described in [35]. This is effective for numerically resolving the coupling of the electric field to ion-concentration due to the relative scale difference in these potentials, namely that applied potential can be on the order of volts while a constant surface charge or potential would result in potentials on the order of tens of millivolts. This approach is modified slightly to include a temperature-dependent permittivity, as gradients in permittivity will affect the electric field profile which correspondingly affects the body-forces on the liquid in the form of dielectric stresses (electrothermal-flows) [28, 36]. Upon decomposing the electric potential into these components, the resulting Poisson equations can be written as (1)–(3)

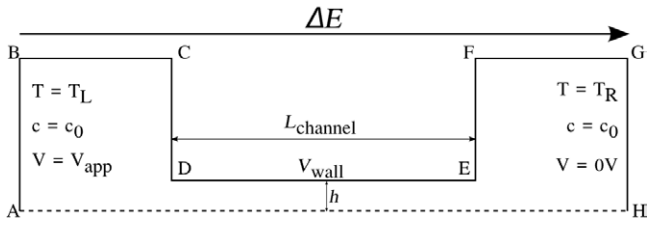

Figure 1. Schematic illustration of the simulation geometry consisting of two reservoirs connected by a nanochannel of half height h.

$$\nabla \cdot (\varepsilon_r \nabla \varphi) = 0 \tag{1}$$

$$\nabla \cdot (\varepsilon_r \nabla \psi) = -\frac{1}{2}(\kappa L_{\text{ref}})^2 (c_1 - c_2) \tag{2}$$

$$\mathbf{E} = -\nabla(\varphi + \psi) \tag{3}$$

In order to obtain dimensionless equivalents, the permittivity was scaled against the permittivity at $T_{\text{ref}} = T_0$, using a linear function of dimensionless temperature, which is a good approximation between 293 and 313 K based on the permittivity (dielectric constant) data of Kaatze (1989) [37], as per [38]. The concentration (c_1 for cation and c_2 for anion) was scaled against bulk concentration in the reservoir $c_{\text{ref}} = c_0$ and the electric potential by scaling against the thermal voltage of an electron $V_{\text{ref}} = k_B T_0/e$. The spatial dimensions were scaled to the channel half-height, i.e. $L_{\text{ref}} = h$, where h is shown in figure 1 as half the total channel height due to the symmetry plane. This allows the space charge density to be scaled against the Debye parameter at $T = T_0$, $\kappa = [(2e^2 z^2 c_0 N_A)/(\varepsilon_{r,0}\varepsilon_0 k_B T_0)]^{1/2}$. All temperature-dependent physical properties are provided in appendix B.

For both cation and anion, the transport balance between convection, diffusion and electromigration can be written in form of the Nernst–Planck equations. For our simulations, we consider the case of a 1:1 electrolyte. In equation (4) the dimensionless diffusivity, D_i, is dependent upon dimensionless temperature, $\theta = (T - T_0)/T_0$. The influence of Soret effects (thermophoresis) was included through the use of the dimensionless ionic heat of transport coefficients (Q_i) for potassium and chloride, taken from Würger (2008) [28, 39]. Soret effects in particular can be significant at lower applied potentials in cases where large temperature gradients exist. The temperature-dependence of individual ion-diffusion coefficients was estimated through temperature dependence of the limiting ion molar conductivity, while diffusivity was considered as independent of concentration over the range of concentrations studied for simplicity [40]. The Péclet number for anion and cation, Pe_{c_i}, is evaluated for the case at the reference temperature.

$$\text{Pe}_{c_i}\mathbf{u} \cdot \nabla c_i = \nabla \cdot D_i \left(\nabla c_i + \frac{c_i Q_i \nabla \theta}{(1+\theta)^2} - \frac{z_i c_i \mathbf{E}}{1+\theta} \right) \tag{4}$$

The dimensionless Navier–Stokes equations are given in (5), with a temperature-dependent viscosity and Coulomb and dielectric body forces. The influence of temperature on the density of solvent, this case water, was neglected as a temperature increase from 293 to 313 K results in a 0.6% change in density while the same temperature range corresponds to a 35% change in viscosity, which motivates treating viscosity as being temperature dependent [41]. Correspondingly the fluid was treated as being incompressible, simplifying both the continuity equation and the viscous dissipation expression.

$$\begin{aligned} \text{Re}(\mathbf{u} \cdot \nabla \mathbf{u}) &= -\nabla p + \nabla \cdot (\mu \nabla \mathbf{u}) + \mathbf{f}_{\text{C}} + \mathbf{f}_{\text{ETF}} = 0 \\ \nabla \cdot \mathbf{u} &= 0 \end{aligned} \tag{5}$$

where $\mathbf{f}_{\text{C}}$ and $\mathbf{f}_{\text{ETF}}$ correspond to the Coulomb and electrothermal force (dielectric force) respectively.

$$\mathbf{f}_{\text{C}} = \frac{k_B T_0 c_0 L_{\text{ref}}}{\mu_0 u_0}(c_1 - c_2)\mathbf{E}$$

$$\mathbf{f}_{\text{ETF}} = -\frac{\varepsilon_0 \varepsilon_{r,0} V_{\text{ref}}^2 L_{\text{ref}}}{2 u_0 \mu_0} |\mathbf{E}|^2 \nabla \varepsilon_r$$

Finally, the system of PDEs is closed by solving for the dimensionless temperature profile via an energy balance (6), where the heat capacity is treated as being essentially constant similar to the arguments given for liquid density whereas the temperature-dependence of thermal conductivity, k, was accounted for. Temperature is scaled relative to the reference temperature $T = T_0$ in the form $\theta = (T - T_0)/T_0$ with T_0 chosen as 293K.

$$\mathbf{u} \cdot \nabla \theta = \frac{1}{\text{Pe}_\theta} \nabla \cdot (k \nabla \theta) + q_{\text{d}} + q_{\text{JH}} \tag{6}$$

The sources of heat generation in the system are from two primary contributions, (i) Joule Heating (q_{JH}), equation (7) via the irreversible dissipation of current into heat and (ii) viscous dissipation (q_{d}), equation (8). JH was evaluated based on the conduction current with the applied electric field, neglecting the contribution of convective current dissipation and the induced electric-field along the nanochannel wall based on order of magnitude analysis [26, 42]. The case of imposed temperature gradients was also considered, to examine the effect on the electrohydrodynamic flows and electrokinetic transport of ions through the nanochannel.

$$q_{\text{JH}} = \left(\frac{\sigma_0 V_{\text{ref}}^2}{\rho C p T_0 u_0 L_{\text{ref}}} \right) \sigma |\nabla \varphi|^2 \tag{7}$$

For an incompressible fluid, the contribution of viscous dissipation can be simplified and non-dimensionalized as follows:

$$q_{\text{d}} = \frac{2 u_0 \mu_0 \mu}{\rho C_p T_0 L_{\text{ref}}} \left[\left(\frac{\partial u}{\partial x} \right)^2 + \left(\frac{\partial v}{\partial y} \right)^2 + \frac{1}{2} \left(\frac{\partial v}{\partial x} + \frac{\partial u}{\partial y} \right)^2 \right] \tag{8}$$

2.2. Simulation details

In order to test the relative influence of various temperature-related phenomena on ion-transport, a microchannel/nanochannel system was considered consisting of two large reservoirs connected via a nanochannel, as illustrated in figure 1. The constriction of the electric field at the nanochannel

throat can potentially play a large role in inducing temperature gradients, due to the high local field gradient as seen for insulator dielectrophoresis [36]. For computational simplicity, a 100× aspect ratio was considered where the nanochannel has a half-plane symmetry height of 1 and a length of 100 dimensionless units. This corresponds to a physical channel dimension of 20 nm and length of 1 μm, of which a 10 nm high half-symmetry is modeled. The reservoirs were chosen as being 200×200 cells ($2\ \mu\text{m} \times 2\ \mu\text{m}$) to try to minimize any potential size effects from concentration polarization or other phenomena. This geometry is conceptually identical to that considered in many papers on isothermal ion-transport nanochannels, such as [25, 33].

The dimensionless equations described were solved numerically using the finite element method (FEM) via the commercial software package COMSOL Multiphysics 5.0. The system geometry is shown in figure 1, with the nanochannel connecting the two reservoirs. The nanochannel was meshed using mapped quadrilateral elements, with 25 000 elements in total in the channel (50×500). The mesh density was arithmetically scaled to account for higher nonlinearities near the walls and entrance/exit effects in the channels, where a higher degree of resolution is required. For solution of the potentials, quadratic Lagrange elements were utilized. For the ion-species concentration and energy balance linear elements and for the Navier–Stokes a P2–P1 velocity/pressure formulation was used.

The boundary conditions tested for simulation cases are provided in appendix A, with a number of conditions tested for temperature and induced electrokinetic potential in general. Specifically, the influence of substrate heat transfer and variation in behaviour for a constant wall potential was considered. In this case, a high constant wall potential could be achieved in a physical nanochannel system using a gated dielectric concept [31, 33], although a constant surface charge is considered more realistic for a conventional nanochannel wall [23, 35]. The influence of temperature on surface charge/potential was neglected in order to simplify the analysis but depending on the specific system may also have significant effects. For a gated nanochannel concept the surface potential is fixed and independent of any temperature effects.

3. Results and discussion

3.1. Isothermal reservoir walls

Initially, the influence of induced heating effects from Joule heating and viscous dissipation in a nanochannel is considered. These effects are assessed for the case where the nanochannel is connected to two large reservoirs with a constant temperature some large distance away from the channel. Local heating effects, especially from corner effects, could potentially give rise to very different local physical properties, affecting the resulting electroosmotic flows from non-electroneutrality as well as induce additional forces upon the fluid in the form of dielectric stresses. It has been reported that viscous dissipation can be significant in nanochannels, giving rise to large temperature gradients which affect the induced electroosmotic flows within the channel [27]. However, in those cases the nanochannel itself was considered as an isolated system without accounting for thermal contact with a much larger reservoir. To investigate the maximum possible local heating in the channel, simulations were run where the channel was connected to reservoirs with $T = T_0$ ($\theta = 0$) external walls, boundary AB and GH in figure 1, and numerically solved at various applied potentials. All other boundaries were considered as insulating/symmetry conditions for temperature.

The initial case considered was that of salt reservoirs at a concentration of 1×10^{-3} M KCl, which corresponds to a Debye length (κ^{-1}, as was defined in section 2.1) of 9.6 nm at each wall and therefore a nearly complete overlap of the nanochannel (20 nm total height). A maximum temperature rise of 0.29 and 0.28 K was observed for a nanochannel with a surface potential of −50 and −100 mV respectively, at an applied electric field strength of 1×10^7 V m^{-1} which represents 10 V across a 1 μm long channel. Compared to this applied field strength, thermophoretic effects are negligible. Similarly, electrothermal flow contributions were negligible compared to the electroosmotic force. At these field strengths, all ion-selectivity in the nanochannel is however lost as the applied field is strong enough to overcome any resistance in the nanochannel. Joule heating provided the bulk of heating at higher applied fields, at lower field strengths viscous dissipation dominated but neither effect was able to generate a local temperature gradient in the system. The convective/diffusive transport of heat into the reservoirs was sufficient in order to suppress localized gradients even in the case of fully insulating walls at all but the highest of applied electric field strengths.

For the case of $c_0 = 1 \times 10^{-2}$ M reservoirs, temperature effects begin to play a larger role even in the case of having a large reservoir with a fixed wall temperature. However, this effect only becomes apparent at quite high applied electric field strengths. For a field strength of 1×10^7 V m^{-1}, simulations showed a maximum temperature rise of 2.8 and 2.7 K was predicted for a surface potential of −50 and −100 mV respectively. The gradient effects even from this larger temperature increase are minimal compared to the direct electrophoretic fluxes and electroosmotic velocity at the double layer. Additionally, this corresponds to very small bulk physical property changes as well. Unsurprisingly, there is also no significant ion-selectivity at field strengths this high (or reservoir salt concentrations this high). The bulk of heating at this field strength came from Joule heating compared to viscous dissipation, which is also the reason behind the near 1 : 1 change in maximum temperature rise and salt concentration comparing the 1×10^{-3} M and 1×10^{-2} M cases. For the simulation cases considered, no significant heating effects could be observed in the case of a connected nanochannel under applied field strengths where the channel still acted as an ion-selective membrane. It is then useful to consider the case of different temperature reservoirs to see what impact temperature effects can have on the resulting system behaviour.

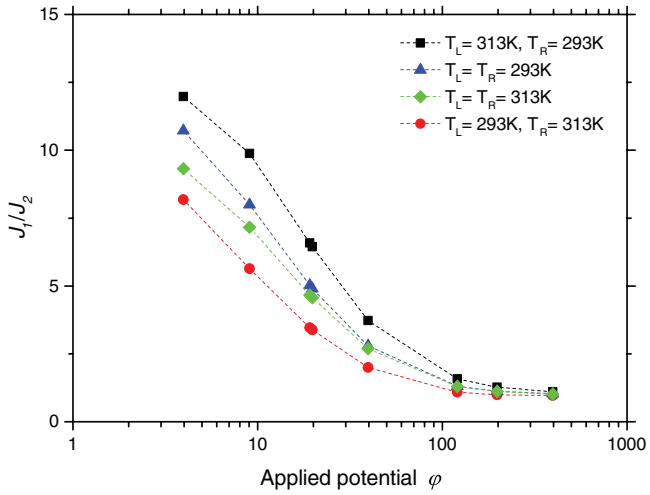

Figure 2. Ion-selectivity, J_1/J_2, for -50 mV gating voltage with different reservoir temperatures, $c_0 = 1 \times 10^{-3}$ M. Lines are for visualization purposes only.

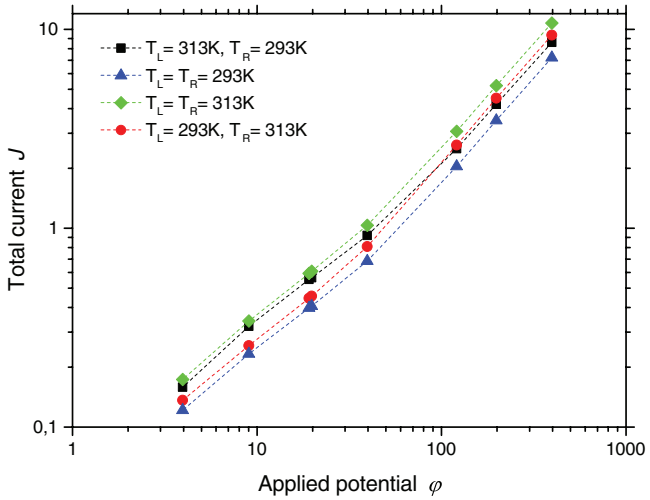

Figure 3. Total current, J_1–J_2, for -50 mV gating voltage with different reservoir temperatures, $c_0 = 1 \times 10^{-3}$ M. Lines are for visualization purposes only.

3.2. Imposed temperature gradient

The case for an isothermal wall or contact with a temperature-regulated reservoir showed minimal temperature variations throughout the system at salt concentrations and field strengths compatible with ion-selectivity. However, imposing a temperature gradient through the use of varying reservoir temperatures could possibly yield interesting couplings between temperature and the induced electrohydrodynamic and electrokinetic behaviour of a microchannel/nanochannel connect with ion-selectivity. In order to study this, the case of (i) imposed negative (high to low) and (ii) positive (low to high) temperature gradients was considered. Case (i) has the temperature gradient in the same direction as the applied electric field and case (ii) has the temperature gradient in the opposite direction.

For case (i), the left-reservoir wall temperature (AB) was set at $T_{\text{left}} = 313$ K while the right was set at $T_{\text{right}} = 293$ K (GH) and for case (ii) this was reversed, with all other boundaries considered as insulating/symmetry conditions, or $\Delta T = -20$ K and 20 K respectively where ΔT is defined as $T_{\text{left}} - T_{\text{right}}$. This effectively imposes a magnitude 20×10^6 K m^{-1} temperature gradient in the x-direction on the system. Conceptually, this is an extension of the case considered by Ghonge *et al* (2013) [28] to include the entrance/exit effects with reservoirs and to study the resulting impact of temperature gradients on the ion-selectivity, flux and electrohydrodynamic flows in the system. These cases are compared to two isothermal cases, namely $T = 293$ K and $T = 313$ K, in order to decouple the effect of varying physical properties for each reservoir and gradient effects. The salt concentration was 1 mM corresponding to a Debye length of 9.6 nm, meaning $\kappa L_{\text{ref}} = 1.04$ and a nearly complete overlap of the nanochannel with the electrical double layer.

The effect of temperature on resulting ion-selectivity (J_1/J_2) and total current (J_1–J_2), where J_i is obtained by integrating the current density (flux in x-direction) over the cross-section of the nanochannel (y-direction), for a -50 mV wall

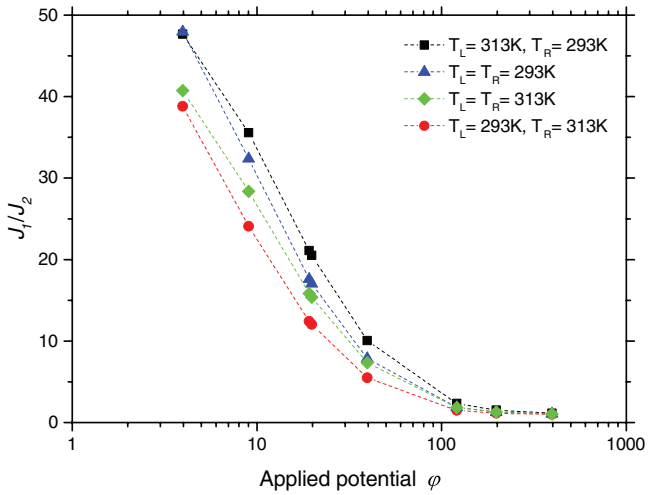

Figure 4. Ion-selectivity, J_1/J_2 for -100 mV gating voltage with different reservoir temperatures, $c_0 = 1 \times 10^{-3}$ M. Lines are for visualization purposes only.

potential are shown in figures 2 and 3 respectively. It can be seen from figure 2 that the ion-selectivity is highest for the negative temperature gradient case (left reservoir is hot, right reservoir is cold) and lowest for the reverse case, while the selectivity for $T = 293$ K is higher than that of $T = 313$ K. For total current, $T = 293$ K represents the lowest total current value at all applied potentials while $T = 313$ K the highest. The negative temperature gradient case had higher flux below a dimensionless potential of $\sim$40 and a lower above compared to the reversed case. Ion-selectivity became negligible above a dimensionless potential of about $\sim$40, which represents a 1×10^6 V m^{-1} applied field strength (1 V across the 1 μm nanochannel).

Similar behaviour is observed for the case of a -100 mV wall potential, as is shown in figures 4 and 5 respectively. It can be seen from figure 4 that the ion-selectivity is again highest for the negative temperature gradient case and lowest for the reverse case, while the selectivity for $T = 293$ K is

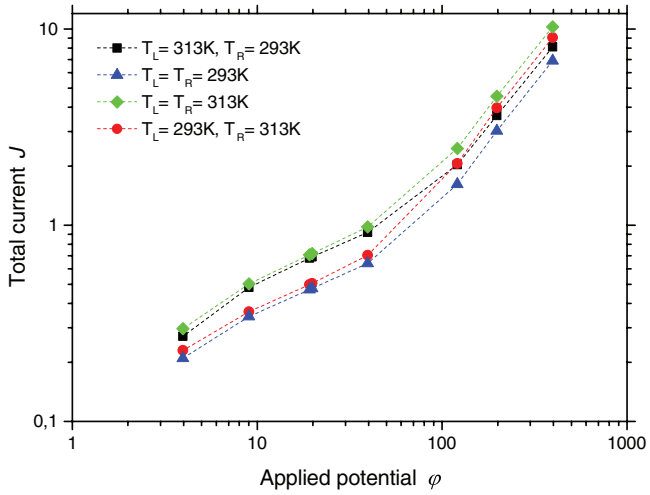

Figure 5. Total current, J_1–J_2, for -100 mV gating voltage with different reservoir temperatures, $c_0 = 1 \times 10^{-3}$ M. Lines are for visualization purposes only.

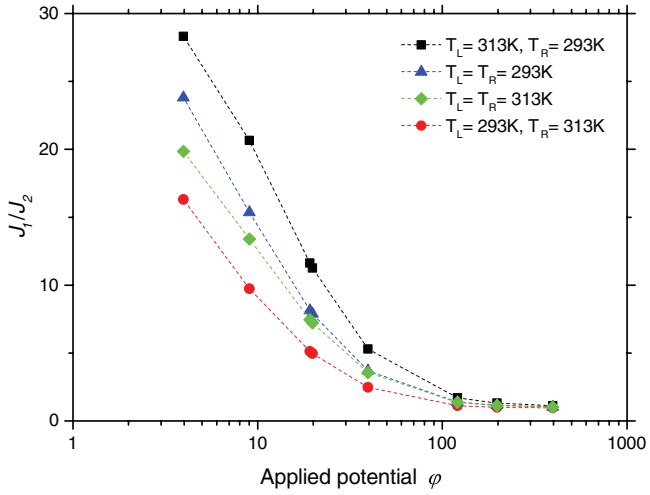

Figure 6. Ion-selectivity, J_1/J_2 for -50 mV gating voltage with different reservoir temperatures, $c_0 = 1 \times 10^{-4}$ M. Lines are for visualization purposes only.

higher than that of $T = 313$ K. Compared to a -50 mV gate, the selectivity is significantly higher. For total current, $T = 293$ K again represents the lowest total current value at all applied potentials while $T = 313$ K the highest. Similar to the -50 mV case, the negative temperature gradient ($\Delta T = -20$ K) case had higher flux below a dimensionless potential of ~40 and a lower above compared to the reversed case ($\Delta T = 20$ K). Ion-selectivity again rapidly decreased above a dimensionless potential of about ~40, although still possessing a higher value compared to the -50 mV case.

For smaller ratios of channel height to electrical double layer ($\kappa L_{\text{ref}} < 1$), i.e. significantly overlapping double layers, the effect of imposed gradients is enhanced further. This is illustrated in figure 6, which shows selectivity results versus applied potential for a reservoir salt concentration of 0.1 mM. This corresponds to Debye length of 33 nm or κL_{ref} of 0.33. Compared to the case with a reservoir salt concentration of 1 mM, the relative change in selectivity between the negative

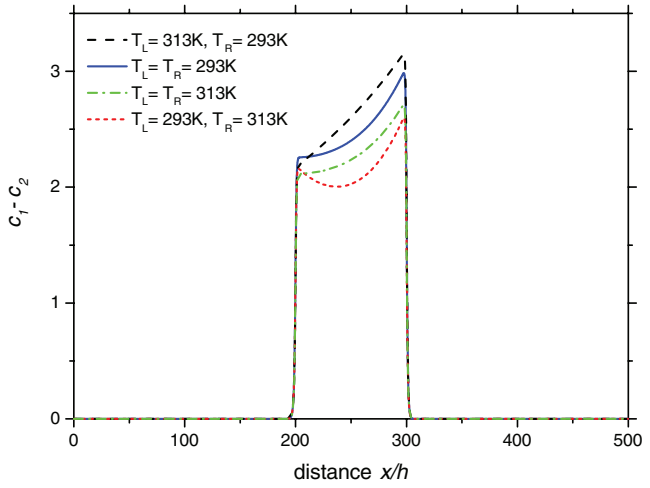

Figure 7. Ion-concentration profile along the mid-line for -50 mV gating voltage with $E_{\text{app}} = 1 \times 10^5$ V m^{-1}, $c_0 = 1 \times 10^{-3}$ M.

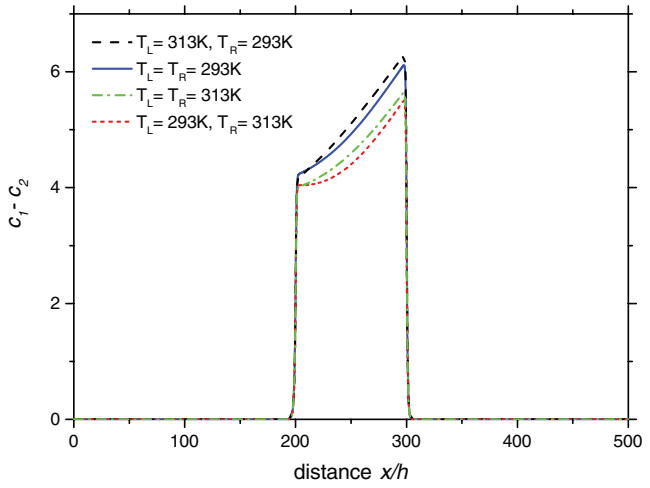

Figure 8. Ion-concentration profile along the mid-line for -100 mV gating voltage with $E_{\text{app}} = 1 \times 10^5$ V m^{-1}, $c_0 = 1 \times 10^{-3}$ M.

and positive temperature gradient case is enhanced for a smaller value of κL_{ref}. This implies that at lower salt concentrations, the effect of temperature gradients/varying reservoir temperatures can become more important for tuning selectivity and ion-transport.

Examination of the concentration difference between cation (c_1) and anion (c_2) along the symmetry mid-line of the system is revealing, showing that there is a large influence from the imposed reservoir temperature difference in the resulting concentration profile for cation and anion. This is illustrated by figures 7 and 8, which show these profiles at an applied field strength of 1×10^5 V m^{-1} and a reservoir salt concentration of $c_0 = 1 \times 10^{-3}$ M. The impact on the cation is more dramatic, as is expected with a negative wall potential where counterions will dominate in the channel. The temperature effects are complicated by the balance between temperature-dependence of physical properties (diffusivity, viscosity and permittivity primarily) and how this effects the resulting fluid flows and electrokinetic transport of ions, which will be elaborated upon later.

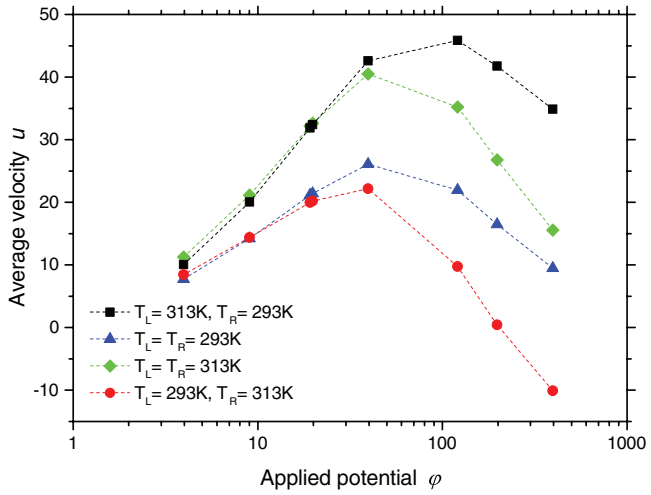

Figure 9. Average velocity in the channel versus potential for -50 mV gating voltage and $c_0 = 1 \times 10^{-3}$ M. Lines are for visualization purposes only.

3.3. Temperature influence on electrohydrodynamics

The influence of temperature on the resulting fluid flow profile is illustrated in figure 9, which shows the average velocity in the nanochannel versus applied potential.

By comparing the average Coulomb force in the channel for the various temperature cases studied, an explanation of the observed flow profile can be provided. For the two cases with identical fixed reservoir wall temperatures, $T = 293$ K and $T = 313$ K, the value of the average Coulomb force is nearly identical. A small decrease at 313 K compared to 293 K is observed for all applied potentials but this is only a few percent at most. The bulk of the increase in velocity is then derived from the decrease in viscosity comparing 293 K with 313 K, which possesses a 35% reduction in viscosity. A higher (positive) electroosmotic velocity is then related to a larger driving force for selectivity, as flows will transport ions from left to right i.e. with the applied field. However, for $T = 313$ K the selectivity is lower compared to $T = 293$ K and this is primarily due to the larger diffusivity of ions meaning larger electromigration forces acting against the resistance of the nanochannel. Since the conductivity in this case is directly proportional to the diffusivity, the $\sim$55% increase in diffusivity between 293 K and 313 K is more substantial for reducing selectivity.

For the imposed reservoir temperature differences, however, large differences exist not only in the viscosity along the channel but in the magnitude of the Coulombic force the fluid experiences. This is owing to the different arrangement of the concentration profiles of cation and anion, which arise from the large dependence of diffusivity, viscosity and permittivity upon temperature. Comparing the case with the temperature gradient in the same direction as the applied field ($\Delta T_x = -20 \times 10^6$ K m^{-1}) versus the reversed direction, the Coulomb force was larger at applied fields above 1×10^5 V m^{-1} and tended to be significantly larger ($\sim$20% or more). For the positive gradient case (ii), an inversion in the flow direction was observed which can be attributed to a stronger increase in diffusivity/conductivity of anion versus cation with temperature as well as induced electrothermal effects. As was previously discussed, at this potential there is no anion-selectivity and in fact anion concentration is slightly higher in the channel again due to the mentioned effect of temperature on diffusivity and electromigration.

3.4. Physical property temperature dependence

In figures 2 and 4, it was shown that imposing a temperature gradient in the same direction as the electric field led to improved selectivity of cations over anions. This was quantified through the ratio of the total cross-sectional flux of cations (J_1) over the cross-sectional flux of anions (J_2). For the case with a negative temperature gradient (temperature gradient in the same direction as electric field), there was an enhancement of selectivity of cation compared to anion which can be explained largely through variations in physical properties.

On the 'hot' reservoir side in the negative temperature gradient case, diffusivity and therefore conductivity are higher compared to the 'cold' side. As was previously discussed, the diffusivity is $\sim$55% higher at 313 K versus 293 K for both anion and cation, meaning the conductivity is also significantly higher. This effectively acts as a barrier for anions to move into the nanochannel on the 'cold' side via diffusion or electromigration and an enhancement for cations to enter on the 'hot' side. The overall balance between these effects also gives rise to a larger effective electrical body force and therefore larger fluid velocity. As was explained earlier, a larger electrohydrodynamic velocity also implies a larger flux of cations from hot to cold and a smaller flux of anions from cold to hot. All of these effects result in a higher degree of ion-selectivity. At applied potentials less than 4 (field strengths less than 1×10^5 V m^{-1}, there are also additional contributions from Soret effects (thermophoretic forces), as is elaborated upon in the next section. As mentioned previously, this selectivity enhancement was observed for both nearly overlapping double layers ($c_0 = 1 \times 10^{-3}$ M) and enhanced for larger double layer overlaps ($c_0 = 1 \times 10^{-4}$ M).

3.5. Temperature gradient effects

The relative influence of the imposed temperature gradient, compared to the effect of different temperatures in each reservoir, on the resulting flux and ion-selectivity depends on the magnitude of the applied potential/electric field. For low applied potentials, the thermophoretic flux of both cation and anion can dominate and will therefore potentially increase or decrease selectivity depending on the ratio of the ionic heat of transport coefficients (Q_i). For example, in case (i) for imposed temperatures considered previously thermophoresis drives both cation and anion in the direction of the applied electric field. Since the ionic heat of transport of potassium is larger than that of chloride (1.064 versus 0.218), this leads to a larger flux of cation compared to anion but both of these thermophoretic forces serve to improve selectivity by driving cations through the nanochannel along with the applied field

and induced electrosmotic velocity and acting against the electrophoretic motion of the anion.

For case (ii), with a positive temperature gradient which is against the applied electric field the opposite is true. Thermophoretic ion flux attempts to drive anions through the nanochannel along with the electrophoretic force, acting to reduce the selectivity relative to the isothermal case at lower applied potentials. However these gradient effects became less significant compared to electrophoretic motion once the applied field was above 1×10^5 V m^{-1}. The average cation thermophoretic flux being $\sim$2% of the electrophoretic flux at this field strength and decreasing with increasing applied potentials.

For the case of imposed temperature gradients, the direct contribution of temperature gradients to fluid forces was considered through the induced dielectric stresses (electrothermal flows). For an imposed temperature gradient with a magnitude of 20×10^6 K m^{-1}, the value of this force in the channel or in the entrance/exit regions to the nanochannel was found to be on average no more than 1% at the highest applied electric field and decreasing in relevance. Essentially, in the case where the Debye layer overlaps or nearly overlaps the channel the Coulombic force acting on the fluid is several orders of magnitude larger compared to the dielectric force generally.

4. Conclusions

In this paper the influence of temperature on the electrohydrodynamic and electrokinetic behaviour in microchannel/nanochannel systems was investigated through a theoretical framework based on a non-isothermal formulation of the Poisson–Nernst–Planck with Navier–Stokes equations. By numerical investigation, the degree of heat generation by Joule heating and viscous dissipation was explored for cases where the nanochannel is in contact with a large reservoir. These effects, as well as the resulting induced flow patterns and ion-transport when a thermal gradient is imposed by having unequal temperature reservoirs, are then quantified.

For the case with a nanochannel in thermal contact with larger microchannel reservoirs, it was found for salt concentrations where there was double layer overlap (ion-selectivity) that no significant local heating gradients could be generated. At these low salt concentrations, Joule heating and viscous dissipation were minimal and thermal dissipation into the reservoirs was able to keep the temperature increase to a minimum. Heating became an issue only at extremely high field strengths (10^7 V m^{-1}), which was well-beyond the region where any degree of ion-selectivity was retained in the system. Higher salt concentrations did show higher degrees of heating, both from Joule heating and from viscous dissipation but this case also did not allow for any degree of ion-selectivity.

When imposing a temperature gradient, much larger effects can be observed. This is through a combination of temperature-related effects, namely the temperature dependence of diffusivity, electrical conductivity, viscosity and permittivity. For the case of ion-transport through a negatively charged nanochannel, an applied temperature gradient in the same direction as the electric field had an enhancing effect on the ion-selectivity primarily from these temperature-dependent properties. At lower applied potentials, the direct effect of temperature gradients in the form of thermophoresis (Soret convection) was also relevant. By reversing this gradient, a decrease in selectivity was obtained. Temperature gradients also had a strong effect on the resulting magnitude of induced fluid flow through the nanochannel, primarily through effecting the electroosmotic force contribution. Electrothermal forces arising from permittivity gradients were found to be negligible for the considered cases where ion-selectivity was maintained.

The results of this work demonstrate the potential benefits from imposed temperature gradients, in terms of improving ion-selectivity, as well how temperature couples to the resulting fluid forces. The cases considered here also demonstrate that for near or completely overlapping Debye layers in nanochannels the influence of Joule heating and viscous dissipation could be neglected and the system can be treated as isothermal at the reservoir temperature in the case of equal temperature reservoirs. It is also of interest for future studies to examine how transport of ion pairs with significantly different diffusion coefficients and temperature-dependence of ion-diffusivities are also affected by such temperature gradients.

Acknowledgments

RGHL acknowledges support from the European Research Council for ERC starting grant 307342-TRAM.

Appendix A. Boundary conditions for simulations

The following boundary conditions were used for each of the boundaries illustrated in figure 1 for the various cases considered. These are identical to the boundary conditions considered in [33] with additional BCs relating to temperature.

AB

Dirichlet/Constant Value for θ, c_i and φ
$\theta = \theta_{\text{left}}$, $c_i = 1$, $\varphi = V_0/V_{\text{ref}}$

Zero Flux for ψ
$\mathbf{n} \cdot (\varepsilon_r \nabla \psi) = 0$

Open Boundary for Velocity
$[-p\mathbf{I} + \mu \nabla \bar{u}]\mathbf{n} = 0$

GH

Dirichlet/Constant Value for θ, c_i and φ
$\theta = \theta_{\text{right}}$, $c_i = 1$, $\varphi = 0$

Zero Flux for ψ
$\mathbf{n} \cdot (\varepsilon_r \nabla \psi) = 0$

Open Boundary for Velocity
$[-p\mathbf{I} + \mu \nabla \bar{u}]\mathbf{n} = 0$

AH

Symmetry Conditions

BC and **FG**

Insulating/Zero Flux for θ, c_i, φ and ψ
Symmetry/No Normal Velocity Component

CD and **EF**

Insulating/Zero Flux for θ and c_i and no-slip $\bar{u} = 0$

DE

Insulating/Zero Flux for θ, c_i and φ

Dirichlet for ψ and u
$\psi = V_{\text{wall}}/V_{\text{ref}}$
$u = 0$

Appendix B. Temperature-dependent physical properties

Temperature-dependent physical properties for permittivity, diffusivity, viscosity and thermal conductivity were used. The diffusivity of individual ion pairs was calculated from molar conductivity data of Benson and Gordon (1945) [40], the permittivity data of Kaatze (1989) [37] and the viscosity and thermal conductivity from the NIST Chemistry Webbook [41]. All physical properties are normalized against the value at 293 K.

$$\varepsilon_r = 1 - 1.2984\theta$$

$$D_1 = 1 + 8.4585\theta$$

$$D_2 = 1 + 8.8466\theta$$

$$\mu = \exp(-6.46\theta)$$

$$k = 1 + 0.8098\theta$$

References

[1] Winter M and Brodd R J 2004 *Chem. Rev.* **104** 4245–70
[2] Dugoeçki P, Gambier A, Nijmeijer K and Wessling M 2009 *Environ. Sci. Technol.* **43** 6888–94
[3] Li Y and Somorjai G A 2010 *Nano Lett.* **10** 2289–95
[4] Kim S J, Ko S H, Kang K H and Han J 2010 *Nat. Nano* **5** 297–301
[5] Nikonenko V V, Kovalenko A V, Urtenov M K, Pismenskaya N D, Han J, Sistat P and Pourcelly G 2014 *Desalination* **342** 85–106
[6] Kim S J, Wang Y C, Lee J H, Jang H and Han J 2007 *Phys. Rev. Lett.* **99** 044501
[7] Jin X, Joseph S, Gatimu E N, Bohn P W and Aluru N R 2007 *Langmuir* **23** 13209–22
[8] Davidson C 2008 Electrokinetic transport in fluidic micro- and nano-channels: a study examining electrokinetic energy conversion and dielectrophoretic particle separation *Masters Thesis* Clemson University, South Carolina, USA
[9] Chang H C, Yossifon G and Demekhin E A 2012 *Annu. Rev. Fluid Mech.* **44** 401–26
[10] Lai C C, Chang C J, Huang Y S, Chang W C, Tseng F G and Chueh Y L 2015 *Nano Energy* **12** 394–400
[11] Chein R, Liao C and Chen H 2010 *Nanoscale Microscale Thermophys. Eng.* **14** 75–94
[12] Chang C C and Yang R J 2010 *Microfluid. Nanofluid.* **9** 225–41
[13] Kim D K, Duan C, Chen Y F and Majumdar A 2010 *Microfluid. Nanofluid.* **9** 1215–24
[14] Inglis D W, Goldys E M and Calander N P 2011 *Angew. Chem. Int. Ed.* **50** 7546–50
[15] Green Y and Yossifon G 2013 *Phys. Rev.* E **87** 033005
[16] Schoch R B and Renaud P 2005 *Appl. Phys. Lett.* **86** 253111
[17] Schiffbauer J and Yossifon G 2012 *Phys. Rev.* E **86** 056309
[18] Rubinstein S M, Manukyan G, Staicu A, Rubinstein I, Zaltzman B, Lammertink R G H, Mugele F and Wessling M 2008 *Phys. Rev. Lett.* **101** 236101
[19] Kim S J, Li L D and Han J 2009 *Langmuir* **25** 7759–65
[20] Yu S, Jeon T J and Kim S M 2012 *Chem. Eng. J.* **197** 289–94
[21] Choi E, Kwon K, Lee S J, Kim D and Park J 2015 *Lab Chip* **15** 1794–8
[22] Durand N F Y and Renaud P 2009 *Lab Chip* **9** 319–24
[23] Van Der Heyden F H J, Stein D and Dekker C 2005 *Phys. Rev. Lett.* **95** 116104
[24] Mani A, Zangle T A and Santiago J G 2009 *Langmuir* **25** 3898–908
[25] Movahed S and Li D 2011 *Electrophoresis* **32** 1259–67
[26] Chen C H 2009 *J. Heat Trans.* **131** 022401
[27] Shi Y, Zhao T S and Guo Z L 2008 *J. Comput. Theor. Nanosci.* **5** 236–46
[28] Ghonge T, Chakraborty J, Dey R and Chakraborty S 2013 *Phys. Rev.* E **88** 053020
[29] Chang C C and Yang R J 2009 *J. Colloid Interface Sci.* **339** 517–20
[30] Chein R and Chung B 2012 *Int. J. Electrochem. Sci.* **7** 12159–80
[31] Zhao C, Song Y and Yang C 2015 *Phys. Fluids* **27** 012003
[32] Cheng L J and Guo L J 2010 *Microfluid. Nanofluid.* **9** 1033–9
[33] Zhao C and Yang C 2014 *Microfluid. Nanofluid.* **18** 785–94
[34] Wang Y, Pant K, Chen Z, Wang G, Diffey W F, Ashley P and Sundaram S 2009 *Microfluid. Nanofluid.* **7** 683–96
[35] Kim K, Kwak H S and Song T H 2011 *Fluid Dyn. Res.* **43** 041401
[36] Hawkins B G and Kirby B J 2010 *Electrophoresis* **31** 3622–33
[37] Kaatze U 1989 *J. Chem. Eng. Data* **34** 371–4
[38] Wood J A, Zhang B, Tomkins M R and Docoslis A 2007 *Microfluid. Nanofluid.* **3** 547–60
[39] Würger A 2008 *Phys. Rev. Lett.* **101** 108302
[40] Benson G C and Gordon A R 1945 *J. Chem. Phys.* **13** 473
[41] Lemmon E, McLinden M and Friend D Thermophysical Properties of Fluid Systems NIST Chemistry WebBook, NIST Standard Reference Database Number 69 eds P J Lindstrom and W G Mallard http://webbook.nist.gov/ (retrieved November 18, 2015)
[42] Coelho P M, Alves M A and Pinho F T 2012 *Microfluid. Nanofluid.* **12** 431–49